Ultrasonics Sonochemistry 21 (2014) 1675–1681

Contents lists available at ScienceDirect

Ultrasonics Sonochemistry

journal homepage: www.elsevier.com/locate/ultson

Low frequency ultrasound (42 kHz) assisted degradation of Acid Blue 113 in the presence of visible light driven rare earth nanoclusters loaded TiO_2 nanophotocatalysts

Panneerselvam Sathishkumar [a,b,*], Ramalinga Viswanathan Mangalaraja [a,*], Oscar Rozas [c], Héctor D. Mansilla [c], M.A. Gracia-Pinilla [d,e], Sambandam Anandan [f]

[a] Advanced Ceramics and Nanotechnology Laboratory, Department of Materials Engineering, Faculty of Engineering, University of Concepcion, Concepcion 407-0409, Chile
[b] Department of Chemistry, Periyar Maniammai University, Vallam, Thanjavur 613403, Tamil Nadu, India
[c] Faculty of Chemical Sciences, University of Concepcion, PO Box 160-C, Correo 3, Concepcion, Chile
[d] Universidad Autónoma de Nuevo León, Facultad de Ciencias Físico-Matemáticas, Av. Universidad, Cd. Universitaria, San Nicolás de los Garza, N.L., Mexico
[e] Universidad Autónoma de Nuevo León, Centro de Investigación e Innovación en Desarrollo de Ingeniería y Tecnología, Avenida Alianza 101 Sur PIIT Monterrey Apodaca, NL 66600, Mexico
[f] Nanomaterials and Solar Energy Conversion Lab, Department of Chemistry, National Institute of Technology, Trichy 620 015, India

ARTICLE INFO

Article history:
Received 26 September 2013
Received in revised form 7 March 2014
Accepted 8 March 2014
Available online 17 March 2014

Keywords:
Rare earth loaded TiO_2
Sonophotocatalysis
Acid Blue 113
Mineralization and combined AOPs

ABSTRACT

An attempt has been made to render the visible light driven photocatalytic activity to the TiO_2 nanocatalysts by loading 1 wt% of rare earth (RE) nanoclusters (Gd^{3+}, Nd^{3+} and Y^{3+}) using a low frequency (42 kHz) producing commercial sonicator. The STEM-HAADF analysis confirms that the RE nanoclusters were residing at the surface of the TiO_2. Transmission electron microscopic (TEM) and X-ray diffraction (XRD) analyses confirm that the loading of RE nanoclusters cannot make any significant changes in the crystal structure of TiO_2. However, the optical properties of the resulted nanocatalysts were significantly modified and the nanocatalysts were employed to study the sonocatalytic, photocatalytic and sonophotocatalytic decolorization as well as mineralization of Acid Blue 113 (AB113). Among the experimented nanocatalysts maximum degradation of AB113 was achieved in the presence Y^{3+}-TiO_2 nanocatalysts. The decolorization of AB113 in the presence and absence of Y^{3+} loaded TiO_2 ensues the following order sonolysis < photocatalysis < sonocatalysis < sonophotocatalysis. The sonophotocatalytic decolorization of AB113 shows 1.4-fold (synergy index) enhanced rate when compared with the two corresponding individual advanced oxidation processes. The sonophotocatalytic mineralization shows that 65% of total organic carbon (TOC) can be removed from AB113 after the 5 h of continuous irradiation however the mineralization cannot be able to show the synergetic effect.

1. Introduction

The nano-size semiconductor photocatalysts are modified using various dopants in order to increase the visible light responsive character of the subsequent nanocatalysts [1–5]. Recently it was reported that the loading of rare earth (RE) dopants into the semiconductor photocatalysts increases the charge imbalance of the resulting nanocatalysts which increased the number of adsorbed hydroxide ions on the surface of the nanocatalysts during the degradation processes and eventually the surface adsorbed hydroxide ions may convert into hydroxyl radicals (·OH) during the degradation of environmental contaminants [6]. Alternatively, it was reported that the loading of RE into the TiO_2 significantly increases the photocatalytic activity through the formation of the complexes between the *f*-orbital of RE dopants with the various organic contaminants which provided an effective environment for the better interaction among the organic contaminants and hydroxyl radicals [7,8]. Therefore, it was expected that the presence of the RE nanoclusters on the surface of the TiO_2 can alter the surface adsorption properties as well as the complexation with the organic contaminants through its *f*-orbital to bring the effective outcome for the environmental remediation. Furthermore, RE nanoclusters act as a sink for the electronic charges to minimize the recombination process during the sonophotocatalysis [9,10].

* Corresponding authors. Address: Advanced Ceramics and Nanotechnology Laboratory, Department of Materials Engineering, Faculty of Engineering, University of Concepcion, Concepcion 407-0409, Chile. Tel.: +56 41 2207389; fax: +56 41 2203391.

E-mail addresses: sathish_panner2001@yahoo.com (P. Sathishkumar), mangal@udec.cl (R.V. Mangalaraja).

http://dx.doi.org/10.1016/j.ultsonch.2014.03.004
1350-4177/

On the other hand, the development of novel methodologies for the purification of water and wastewater released from the industrial sectors is essentially required in order to reduce the existing operating cost [11–13]. Concurrently, the modification or replacement of the expensive components from the existing technology can also make the degradation process cost-effective for the commercial applications [14–17]. The extended utilization of a low frequency ultrasound (42 kHz) for the degradation of recalcitrant organic contaminants reduces the operating cost of the sonication process. However the rate of low frequency assisted removal of organic pollutants is diminutive when compared with the high frequency supported sonication processes. Therefore the adaptation of other advanced oxidation process (AOP) such as photocatalysis with the 42 kHz assisted sonicator makes the sonophotocatalysis process more effective for the removal of organic contaminants [18,19]. The development of visible light responsive photocatalysts for the degradation of various organic contaminants is of current interest which further reduces the operating cost [20–23].

Furthermore, the RE doping could control the TiO_2 particle growth, crystal transformation, and cause negative shift of the conduction band, and thus increase the resulting photocatalytic activity of the nanocatalysts [24,25]. Therefore, based on the previous studies and the necessity to evaluate the sonophotocatalytic efficiency of the various RE dopants, in this study Gadolinium (Gd^{3+}), Neodymium (Nd^{3+}) and Yttrium (Y^{3+}) were loaded into the TiO_2 nanocatalysts by a simple low frequency assisted sonochemical process. The resulted nanophotocatalysts were employed to evaluate the sonocatalytic, photocatalytic, and sonophotocatalytic degradation of Acid Blue 113 (AB113). The elemental Yttrium was located in the "d block elements" of the modern periodic table however it shows the chemically equal character with the rare earth elements therefore, Y^{3+} was considered as a RE dopant in this study and the resulted catalytic activity was taken into account to compare with other RE dopants.

2. Experimental

2.1. Materials and methods

Titanium dioxide nanopowder and nitrates of Gadolinium (Gd), Neodymium (Nd) and Yttrium (Y) were purchased from Sigma–Aldrich and used as the starting materials for the preparation of rare earth doped TiO_2 nanocatalysts. Acid Blue 113 (diazo dye, $C_{32}H_{21}N_5Na_2O_6S_2$; C.I. 26360) was received from Sigma–Aldrich and used without further purification. Unless otherwise specified, all reagents used were of analytical grade and the solutions were prepared using double distilled water. The particle size of the prepared nanoparticles was calculated from the X-ray diffraction data (Philips PW1710 diffractometer, CuKα radiation, Holland) using Scherrer equation. Surface morphology, particle size, and various contours of the nanocatalyst powders were analyzed by Transmission Electron Microscopy (FEI TITAN G2 80-300) operated at 300 KeV. Diffuse reflectance UV–Vis spectra of the nanocatalysts were recorded using a Shimadzu 2550 spectrophotometer equipped with an integrating sphere accessory employing $BaSO_4$ as reference material. Photoluminescence (PL) spectra were recorded using a Shimadzu RF-5301 spectrofluorophotometer. The surface area, pore volume and pore diameter of the samples were measured with the assistance of Flowsorb II 2300 of Micrometrics, Inc. The total organic carbon (TOC) for all the samples was analyzed by direct injection of the filtered sample solutions into a TOC analyzer (Vario TOC cube, Cientec Instrumentos S.A). Prior to the analysis, the instrument was calibrated with potassium hydrogen phthalate. TOC_0 is the TOC measured after the equilibrium adsorption of the dye on the nanocatalysts surface and TOC obtained at various irradiation times is denoted as TOC_t.

2.2. Preparation of nanocatalysts

The nitrate precursors (1 mol%) of rare earth metals (Gd^{3+}, Nd^{3+} and Y^{3+}) was added to the 100 ml aqueous suspension containing one gram of TiO_2 and stirred for 30 min. The suspension was irradiated with ultrasound (42 kHz) continuously for 2 h at room temperature then filtered and the solids were redispersed in 100 ml of distilled water under vigorous stirring (1200 rpm) for 15 min at 50 °C. The above procedure was repeated several times and then dried at 110 °C for 12 h followed by calcination at 550 °C for 5 h in order to get pure nanocatalysts. Similarly the bare TiO_2 was treated using the same methodology and calcinated at 550 °C for comparison.

2.3. Photocatalysis and sonophotocatalysis

A desired concentration of AB113 was prepared by dissolving the appropriate amount of dye in 250 ml of water and 250 mg of nanocatalysts (RE-TiO_2/TiO_2) was added to the dye solution. The degradation of Acid Blue 113 (AB113) was studied under ambient atmospheric conditions and at natural solution pH (~6.0). In order to ensure the adsorption/desorption equilibrium, the dye/nanocatalyst slurry was stirred for 45 min in dark condition prior to irradiation. After that, the lamp and/or the sonicator were turned on and this was taken as "time zero" for the degradation reactions. The photocatalytic studies were performed using a light source (Cole-Parmer, USA) illuminating spectral range ⩾ 420 nm with the intensity of incident irradiation ⩾ 100000 ± 100 Lux measured by Lux meter (Cole-Parmer, USA). All the sonochemical reactions in this study were carried out by using a commercially available sonicator (8890, Cole-Parmer, USA) producing 42 kHz ultrasonic waves. The experimental setup and conditions used for photolysis, sonolysis, and sonophotolysis were identical. During the degradation studies, the target substance (organic contaminants) was

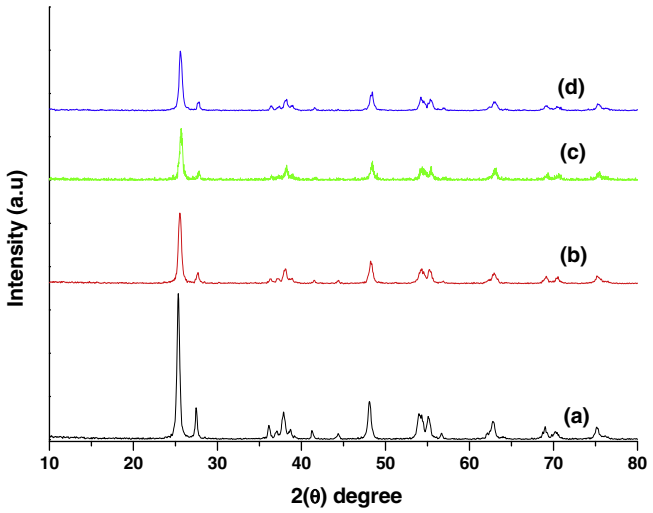

Fig. 1. X-ray diffraction pattern of bare (a) and RE ((b) Gd^{3+}, (c) $Nd^{3+}$and (d) Y^{3+} loaded TiO_2 nanocatalysts.

Table 1
Physicochemical characteristics of RE loaded TiO_2 nanocatalysts.

S. No	Nanophotocatalyst	Surface area (S_{BET} m^2/g)	Band gap (eV)
1	TiO_2	44.27	3.2
2	Nd^{3+}-TiO_2	47.98	2.67
3	Gd^{3+}-TiO_2	46.42	2.69
4	Y^{3+}-TiO_2	45.09	2.65

sonicated in the presence and absence of catalysts and visible light. The apparent kinetics of disappearance of the substrate (AB113) was determined by following the concentration of the substrate (λ_{max} = 574 nm) using Shimadzu UV–Vis 2550 spectrophotometer. Prior to the analysis, the nanocatalysts were separated from the suspension by using a 0.45 μm Polytetrafluoroethylene (PTFE) filter.

3. Results and discussion

3.1. Characterization of the nanocatalysts

The X-ray diffraction patterns of the pure and RE loaded TiO_2 nanocatalysts are shown in Fig. 1, which clearly indicate that the loading of RE cannot make any significant changes in the crystal structure of TiO_2, thus ruled out the possibility of replacing the Ti^{4+} ions by the RE^{3+} ions [25]. However, the observed decrease in the diffractogram intensity of the RE loaded TiO_2 compared with pure TiO_2 evidently suggests that the loaded RE^{3+} ions may dwell on the surface rather than penetrating into the crystal structure of the TiO_2. Concomitantly the lowering of crystallite size was noticed from the diffractograms of the RE loaded TiO_2 when compared with the pure TiO_2 (Fig. 1) indicates that the surface area of the RE loaded TiO_2 nanocatalysts might be increased. Nevertheless the catalytic performance of the pure and RE loaded nanocatalysts was depended on the effective surface area of the synthesized nanocatalysts [3]. The surface area (S_{BET}) of the pure and RE loaded TiO_2 nanocatalysts were measured and presented in Table 1. The RE loaded TiO_2 significantly shows the increased surface area when compared with the bare TiO_2. The increased surface area of RE loaded TiO_2 nanocatalysts clearly illustrates that the ionic radius of the RE dopants significantly suppressed the diffusion into the crystal matrix of the TiO_2 [24].

Fig. 2 shows the representative scanning transmission electron microscopy coupled with high-angle annular dark-field (STEM-HAADF) images of the bare and RE loaded TiO_2 nanocatalysts. From the micrographs, the RE nanoclusters can be easily identified at the surface of the nanocatalysts (Fig 2a–c) and the size of the nanoclusters can be calculated ~1 nm over the surface of the TiO_2. It can be concluded that the penetration of RE nanoclusters cannot be supported by the present experimental conditions which significantly supports the observation made from the XRD and BET analyses. In addition, the presence of the nanoclusters could improve the separation of electronic charges during the visible light excitation of the nanocatalysts. Moreover, the existence of the RE nanoclusters at the TiO_2 surface may expect to reduce the band gap from 3.2 eV. The HRTEM analysis shows the high crystallinity of the bare and RE loaded TiO_2 nanocatalysts and the fringe spacing of 0.35 nm can be indexed to (1 0 1) plane of anatase TiO_2 (Fig. 3). The bright grey particles in the TEM micrographs are obviously the nanoparticles of TiO_2 and the RE nanoclusters have been observed as the dark patches on the grey surface of TiO_2. On the other hand the presence of RE dopants prevented adhering of the TiO_2 nanoparticles. The particle size calculated for the RE loaded TiO_2 from the HRTEM and STEM-HAADF analysis shows 20 ± 3 nm which is in consistent with the particle size calculated from the XRD analysis.

The solid state photoluminescence (PL) spectra of pure and RE loaded TiO_2 nanocatalysts measured at room temperature are presented in Fig. 4. Generally, pure TiO_2 exhibits four shallow trap levels at 2.80, 2.70, 2.56, and 2.34 eV in the PL spectrum which is due

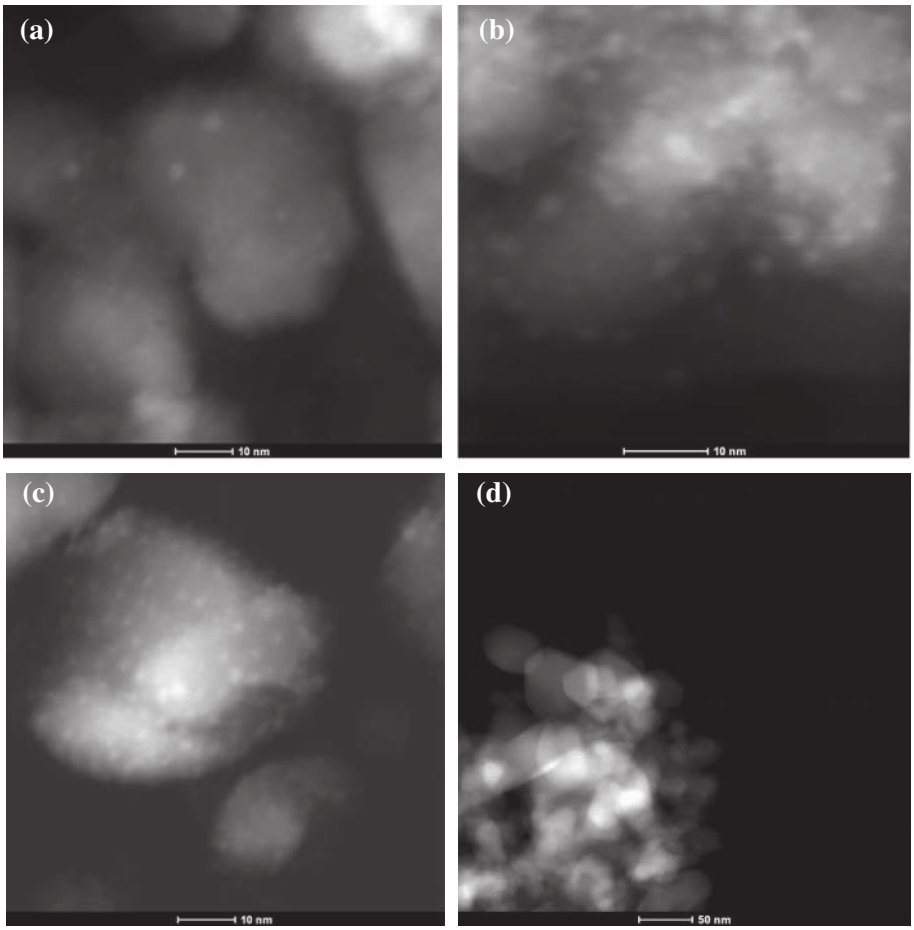

Fig. 2. STEM-HAADF images of (a) Gd^{3+}, (b) $Nd^{3+}$and (c) Y^{3+} loaded TiO_2 nanocatalysts and (d) corresponds to the bare TiO_2.

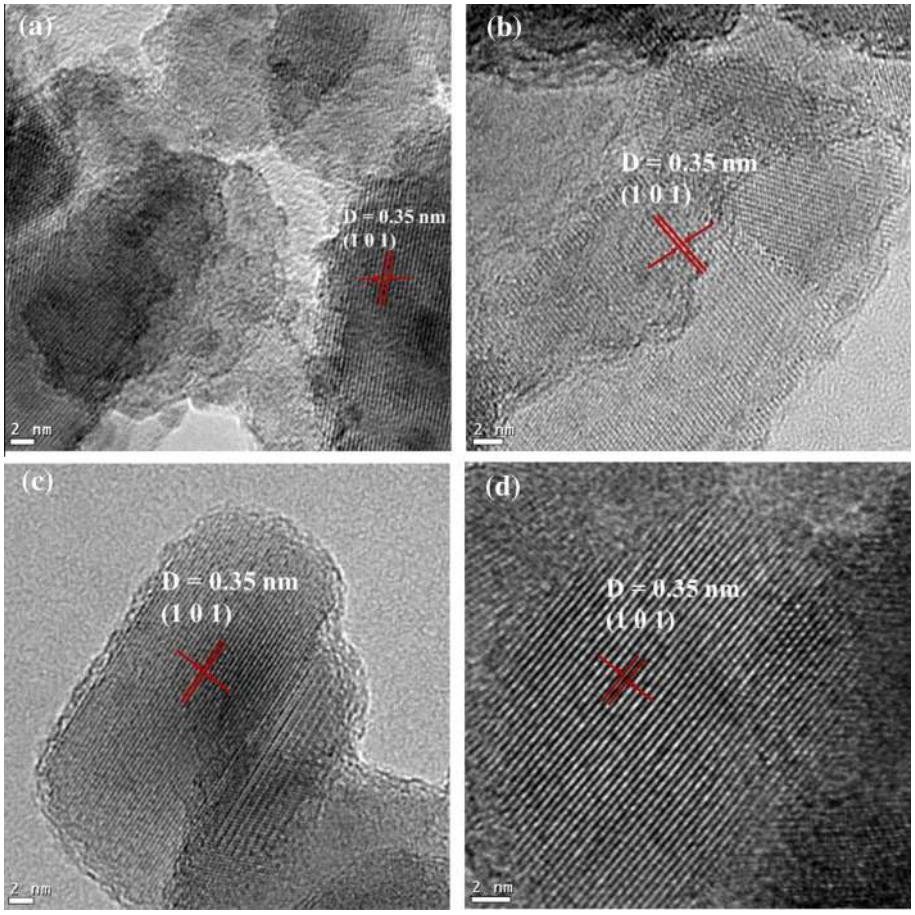

Fig. 3. HRTEM micrographs of (a) Gd^{3+}, (b) Nd^{3+} and (c) Y^{3+} loaded TiO_2 nanocatalysts and (d) corresponds to the bare TiO_2.

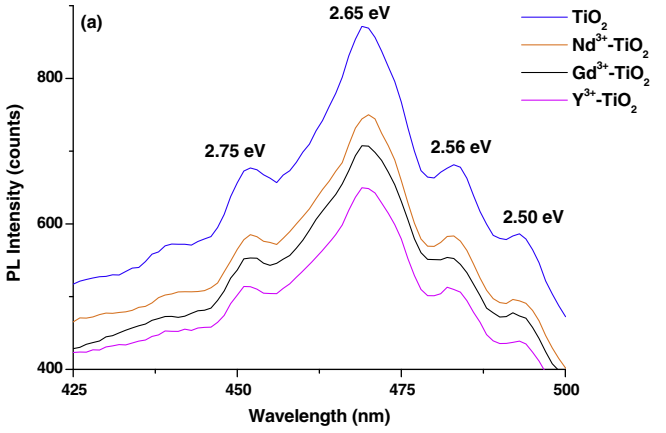

Fig. 4. Emission spectrum of the various nanocatalysts excited at 275 nm.

to the characteristic emission of the oxygen vacancies present in the bare TiO_2 [26]. In the present study, the PL values (2.75, 2.65, 2.56 and 2.50 eV) measured when the synthesized nanocatalysts underwent 275 nm excitation at room temperature which may slightly vary from the pure TiO_2 (Fig. 4). The observed difference in the shallow trap position may due to the difference in the experimental conditions adopted for the synthesis and the resulting size of the nanocatalysts [26,27]. The band gap excitation at 345 nm of the bare and RE loaded TiO_2 nanocatalysts emanated the characteristic emission peak at 390 nm which belongs to the anatase phase of TiO_2 nanocatalysts [28] and the appearance of the characteristic peak in all the synthesized nanocatalysts confirms that there is no phase change was occurred. However the RE loaded TiO_2 nanocatalysts excited at 345 nm and 365 nm show the lower PL intensity when compared with the bare TiO_2 (data not shown). The lower PL intensity clearly illustrates that the low radiative recombination of the electronic charges which are generated during the excitation of the RE-TiO_2.

Further, the optical properties of pure and RE-TiO_2 nanocatalysts were studied using diffuse reflectance UV–Vis (DR-UV–Vis) analysis (Fig. 5). The optical band edge shift from ~390 nm was noticed in all the nanocatalysts which suggest that the loading of RE nanoclusters had been occurred preciously by the sonochemical treatment adopted in the preparation processes. The absorption edge shifts to a longer wavelength in the order of [Gd^{3+} < Nd^{3+} < Y^{3+}]-TiO_2 when compared with the pure TiO_2. The attributed red shift was due to the charge transfer transition between the rare earth ion "f electron" and the "conduction or valance band of TiO_2" [29]. The Nd^{3+} loaded TiO_2 had three typical absorption peaks in its DR-UV–Vis spectrum located at 527, 586 and 762 nm which are corresponding to the various transitions between the guest and host materials [30]. In the case of Gd^{3+} and Y^{3+} loaded TiO_2 there was no characteristic absorption observed in the DR-UV–Vis spectrum however significant changes in the optical band edge was noticed. The band gap of the prepared nanocatalysts was calculated from the DR-UV–Vis spectrum using Tauc plot derived from Kubelka–Munk function (Fig. 6). The RE-TiO_2 nanocatalysts significantly show lower band gap than the bare TiO_2 (Table 1), therefore all the RE loaded TiO_2 nanocatalysts are expected to oxidize the organic contaminants in the presence of visible light or sunlight.

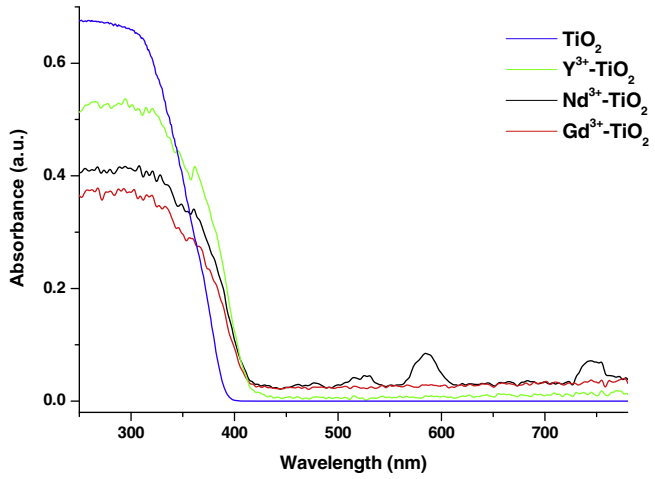

Fig. 5. Diffuse reflectance UV–Vis (DR-UV–Vis) analysis of bare and RE loaded TiO_2 nanocatalysts.

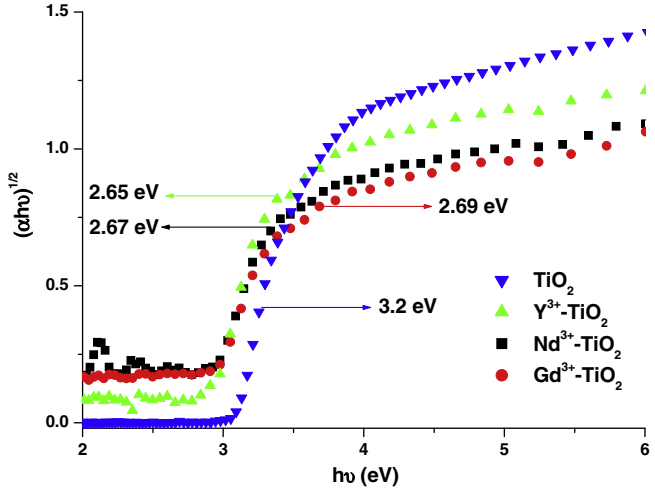

Fig. 6. The Tauc plot derived from the Kubelka Munk function for the various nanocatalysts using DR UV–Vis spectrum.

3.2. Degradation of AB113 using RE loaded TiO_2 nanoparticles

Sonolytic, sonocatalytic, photocatalytic and sonophotocatalytic decolorization and mineralization of Acid Blue 113 (AB113) were carried out at the fixed initial concentration of AB113 (1×10^{-5} M) and nanocatalyst (RE-TiO_2/TiO_2) (1 g/L) in order to achieve the maximum catalytic efficiency of the nanocatalysts. The kinetics of decolorization was followed at the maximum absorption of AB113 (λ_{max} = 574 nm) using the UV–Vis spectrophotometer (Shimadzu 2550). The rapid decolorization of AB113 was not observed during the sonolysis (0.0037×10^{-5} s^{-1}) since the proficiency of sonolysis process suffers to oxidize the dye molecules. However, the sonocatalytic decolorization of AB113 showed somewhat enhanced rate (0.91×10^{-5} s^{-1}) when compared to sonolysis of AB113. The solid support (nanocatalysts) provided an effective environment for the effective interaction of organic contaminants with the free radicals produced from the sonolysis which tends to achieve the enhanced sonocatalytic degradation when compared with the rate achieved from the sonolysis. In the photocatalytic processes, the observed decrease in C/C_0 with respect to the irradiation time indicates the decolorization of AB113 ensues only in the presence of nanocatalysts whereas there is no decolorization was observed during the photolysis and in the dark conditions (absence of light and/or nanocatalysts). In order to make the comparison of the sonophotocatalytic activity of the synthesized nanocatalysts, the corresponding rate constants are plotted against the various nanocatalysts with respect to the fixed initial concentrations [AB113 (1×10^{-5} M) and RE-TiO_2 (1 g/L)] as shown in Table 2. The apparent rate constants observed for the various rare earth nanoclusters (RE) loaded TiO_2 significantly show higher sonophotocatalytic activity than the bare TiO_2. Particularly, Y^{3+} loaded TiO_2 shows the maximum sonophotocatalytic activity when compared with Gd^{3+} and Nd^{3+} loaded TiO_2 (Table 2). The reason for the attained maximum sonophotocatalytic activity can be evidenced from DR-UV–Vis analysis which shows the maximum red shift and the smaller band gap (2.65 eV) for Y^{3+} loaded TiO_2 when compared with the Nd^{3+} and Gd^{3+} loaded TiO_2. In addition, the presence of ultrasound enhances the possibility of the effective interaction of AB113 with the electronic charges generated during the catalytic processes. Therefore the maximum charge carrier initiation was achieved during the sonophotocatalytic degradation of AB113 in the presence Y^{3+}-TiO_2 nanophotocatalysts.

Table 2
Degradation rate constant of obtained for different processes using [nanocatalyst] = 1 g/L and [AB113] = 1×10^{-5} M.

S. No	Process	Nanocatalyst	Rate, 10^{-5} s^{-1}
1	Photocatalysis	TiO_2	0.21
2	Sonocatalysis		5.32
3	Sonophotocatalysis		7.25
4	Photocatalysis	Y^{3+}-TiO_2	4
5	Sonocatalysis		8.8
6	Sonophotocatalysis		18
7	Sonophotocatalysis	Gd^{3+}-TiO_2	15.12
8	Sonophotocatalysis	Nd^{3+}-TiO_2	13.05

To compare the sonocatalytic, photocatalytic and sonophotocatalytic efficacy of Y^{3+}-TiO_2, the degradation of AB113 was carried out at the fixed initial concentrations as shown in Table 2. The sonophotocatalytic degradation of AB113 was reached the maximum rate of decolorization when compared with the sonocatalytic and photocatalytic decolorization processes. The sonophotocatalytic degradation shows the 1.4-fold enhanced rate of decolorization of AB113 when compared with the two individual sonocatalytic and photocatalytic processes. The observed synergy index values > 1 indicate that the combined process exceeds the sum of the separate advanced oxidation processes. However the synergy index of 1.4 indicating a slight synergistic effect for the sonophotocatalytic process in the presence of Y^{3+} loaded TiO_2 whereas only an additive effect was observed in the presence of bare TiO_2. The synergy index for the combination of two individual advanced oxidation processes (AOPs) depends on the numerous experimental factors [31,32]. The reason for the enhanced sonophotocatalytic degradation was the continuous scrubbing of the AB113 and its derivatives from the nanocatalyst surface by the ultrasound. Besides the enhanced generation of the intermediate species such as singlet oxygen ($^1O_2$) and superoxide ($O_2^{\cdot}$) radicals and hydroxyl radicals during the sonophotocatalytic degradation is an additional factor for the enhanced decolorization of AB113 [20]. On the other hand, ultrasound directs the generation and migration of holes from the nanocatalysts to the bulk solution to provide the superior environment for the decolorization of AB113 [33]. Therefore the recombination of electronic charges is diminished and the enhanced rate of decolorization of AB113 was achieved for the sonocatalysis and sonophotocatalysis processes rather than photocatalysis.

The total organic carbon (TOC) analysis of AB113 was carried out for the various advanced oxidation processes for 5 h continuously and presented in Fig. 7. The TOC removal allows the following order for the mineralization of AB113 in the presence

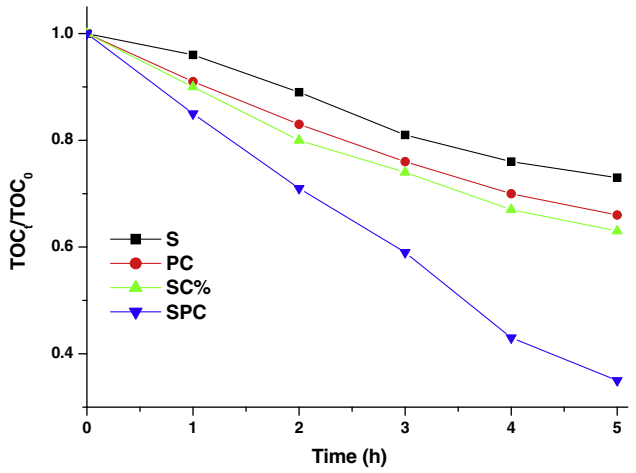

Fig. 7. Total organic carbon (TOC) removal of AB113 during various advanced oxidation processes ((S) sonolysis, (PC) photocatalysis, (SC) sonocatalysis and (SPC) sonophotocatalysis) in the presence and absence of Y^{3+} loaded TiO_2.

and absence of Y^{3+}-TiO_2, sonolysis < photocatalysis < sonocatalysis < sonophotocatalysis. The maximum rate of mineralization (65%) was attained by the sonophotocatalytic process which resembles the similar trend observed during the decolorization process. Further, it can be evidenced from the Fig. 7 that the sonophotocatalytic mineralization of AB113 cannot be able to show any synergetic effect as it was obtained from the decolorization process however the combinatorial effect of the two AOPs namely sonocatalysis and photocatalysis was attained during the mineralization. The synergetic effect during the decolorization was observed based on the concentration of –N=N– moiety present in the dye molecule whereas the TOC was calculated from the sonophotocatalytic oxidation of carbon atoms into CO_2 from the AB113. The intermediates produced during the sonophotocatalytic mineralization are responsible for the additive effect since the free radical attacking positions or the possibility of hydroxylated intermediates production get decreased from the intermediates when compared with the parent compounds [34–37]. Further, the initial concentration of AB113 was changed from its fixed concentration and the number of active surface area per gram of Y^{3+}-TiO_2 decreases since the active surface area of the nanocatalysts were eventually occupied by the dye and its intermediate molecules even if the nanocatalysts were cleaned continuously by the ultrasound.

4. Conclusion

The rare earth nanoclusters were loaded into surface of the TiO_2 using a simple, convenient and efficient low frequency assisted sonochemical method to fetch the visible light induced photocatalytic activity to the resulting nanocatalysts. In addition to that, a simple and low frequency (42 kHz) producing ultrasonic equipment was attached to the photocatalytic reactor to carry out the sonolysis, sonocatalytic and sonophotocatalytic degradation of AB113. The RE loaded TiO_2 nanocatalysts were characterized using various analytical techniques to show that the loading of RE is not affected the crystal and morphological phase of TiO_2 nevertheless the loading influenced the photocatalytic behavior of TiO_2. The Y^{3+}-TiO_2 showed the maximum photocatalytic, sonocatalytic and sonophotocatalytic degradation of AB113 among the various nanocatalysts utilized in this study. The RE dopant loaded to the TiO_2 nanocatalysts acts as the center for the recombination of electronic charges however the slight increase in the dopant concentration could modify the resulting photocatalytic activity of the respective nanocatalysts. On the other hand the surface adsorbed hydroxyl ions, oxygen vacancies and oxidation state of oxides played the major role for the enhanced photocatalytic activity of Y^{3+}-TiO_2.

Acknowledgements

The authors would like to thank FONDECYT Postdoctorado project No. 3120095 and FONDECYT No. 1130916 Government of Chile, Santiago, for financial assistance.

References

[1] J. Cao, X. Li, H. Lin, B. Xu, S. Chen, Q. Guan, Surface acid etching of $(BiO)_2CO_3$ to construct $(BiO)_2CO_3$/BiOX (X = Cl, Br, I) heterostructure for methyl orange removal under visible light, Appl. Surf. Sci. 266 (2013) 294–299.
[2] C. Hengky, X. Moya, N.D. Mathur, S. Dunn, Evidence of high rate visible light photochemical decolourisation of Rhodamine B with $BiFeO_3$ nanoparticles associated with $BiFeO_3$ photocorrosion, RSC Adv. 2 (2012) 11843–11849.
[3] P. Sathishkumar, R.V. Mangalaraja, S. Anandan, M. Ashokkumar, Photocatalytic degradation of ternary dye mixture in aqueous environment using gold nanoparticles loaded amino and mercapto functionalized TiMCM-41 nanocatalysts in the presence of visible light, Sep. Purif. Technol. 102 (2013) 67–74.
[4] P. Sathishkumar, N. Pugazhenthiran, R.V. Mangalaraja, A.M. Asiri, S. Anandan, ZnO supported $CoFe_2O_4$ nanophotocatalysts for the mineralization of Direct Blue 71 in aqueous environments, J. Hazard. Mater. 252–253 (2013) 171–179.
[5] N. Pugazhenthiran, P. Sathishkumar, P. Maruthamuthu, S. Anandan, HPA immobilized on the functionalized Ti-MCM-41 nanochannels for photocatalytic degradation of ternary azo dye effluents, J. Porous Mater. 20 (2013) 489–499.
[6] S. Bingham, W.A. Daoud, Recent advances in making nano-sized TiO_2 visible-light active through rare-earth metal doping, J. Mater. Chem. 21 (2011) 2041–2050.
[7] K.T. Ranjit, I. Willner, S.H. Bossmann, A.M. Braun, Lanthanide oxide doped titanium dioxide photocatalysts: effective photocatalysts for the enhanced degradation of salicylic acid and t-cinnamic acid, J. Catal. 204 (2001) 305–313.
[8] K.T. Ranjit, I. Willner, S.H. Bossmann, A.M. Braun, Lanthanide oxide-doped titanium dioxide photocatalysts: novel photocatalysts for the enhanced degradation of p-chlorophenoxyacetic acid, Environ. Sci. Technol. 35 (2001) 1544–1549.
[9] Z.M. El-Bahy, A.A. Ismail, R.M. Mohamed, Enhancement of titania by doping rare earth for photodegradation of organic dye (Direct Blue), J. Hazard. Mater. 166 (2009) 138–143.
[10] Q. Xiao, Z.C. Si, Z.M. Yu, G.Z. Qiu, Sol–gel auto-combustion synthesis of samarium-doped TiO_2 nanoparticles and their photocatalytic activity under visible light irradiation, Mater. Sci. Eng. B 137 (2007) 189–194.
[11] Y.G. Adewuyi, Sonochemistry in environmental remediation. 2. Heterogeneous sonophotocatalytic oxidation processes for the treatment of pollutants in water, Environ. Sci. Technol. 39 (2005) 8557–8570.
[12] Y.G. Adewuyi, Sonochemistry in environmental remediation. 1. Combinative and hybrid sonophotochemical oxidation processes for the treatment of pollutants in water, Environ. Sci. Technol. 39 (2005) 3409–3420.
[13] C. Drosou, A. Coz, N.P. Xekoukoulotakis, A. Moya, Y. Vergara, D. Mantzavinos, Peracetic acid-enhanced photocatalytic and sonophotocatalytic inactivation of *E. coli* in aqueous suspensions, J. Chem. Technol. Biotechnol. 85 (2010) 1049–1053.
[14] N.N. Mahamuni, Y.G. Adewuyi, Advanced oxidation processes (AOPs) involving ultrasound for waste water treatment: a review with emphasis on cost estimation, Ultrason. Sonochem. 17 (2010) 990–1003.
[15] Y. Wang, D. Zhao, W. Ma, C. Chen, J. Zhao, Enhanced sonocatalytic degradation of azo dyes by Au/TiO_2, Environ. Sci. Technol. 42 (2008) 6173–6178.
[16] P.R. Gogate, S. Mujumdar, A.B. Pandit, A sonophotochemical reactor for the removal of formic acid from wastewater, Ind. Eng. Chem. Res. 41 (2002) 3370–3378.
[17] I.M. Khokhawala, P.R. Gogate, Degradation of phenol using a combination of ultrasonic and UV irradiations at pilot scale operation, Ultrason. Sonochem. 17 (2010) 833–838.
[18] P.R. Gogate, A.B. Pandit, Sonophotocatalytic reactors for wastewater treatment: a critical review, AIChE J. 50 (2004) 1051–1079.
[19] L.H. Thompson, L.K. Doraiswamy, Sonochemistry: science and engineering, Ind. Eng. Chem. Res. 38 (1999) 1215–1249.
[20] S. Kaur, V. Singh, Visible light induced sonophotocatalytic degradation of Reactive Red dye 198 using dye sensitized TiO_2, Ultrason. Sonochem. 14 (2007) 531–537.
[21] K. Zhang, W. Oh, Kinetic study of the visible light-induced sonophotocatalytic degradation of MB solution in the presence of Fe/TiO_2-MWCNT catalyst, Bull. Korean Chem. Soc. 31 (2010) 1589–1595.
[22] B. Neppolian, L. Ciceri, C.L. Bianchi, F. Grieser, M. Ashokkumar, Sonophotocatalytic degradation of 4-chlorophenol using Bi_2O_3/$TiZrO_4$ as a visible light responsive photocatalyst, Ultrason. Sonochem. 18 (2011) 135–139.

[23] C.G. Joseph, G.L. Puma, A. Bono, D. Krishnaiah, Sonophotocatalysis in advanced oxidation process: a short review, Ultrason. Sonochem. 16 (2009) 583–589.
[24] J.H. Li, X. Yang, X.D. Yu, L.L. Xu, W.L. Kang, W.H. Yan, H.F. Gao, Z.H. Liu, Y.H. Guo, Rare earth oxide-doped titania nanocomposites with enhanced photocatalytic activity towards the degradation of partially hydrolysis polyacrylamide, Appl. Surf. Sci. 255 (2009) 3731–3738.
[25] A.W. Xu, Y. Gao, H.Q. Liu, The preparation, characterization, and their photocatalytic activities of rare-earth-doped TiO_2 nanoparticles, J. Catal. 207 (2002) 151–157.
[26] N.D. Abazovic, M.I. Cyomor, M.D. Dramicanin, D.J. Jovanovic, S.P. Ahrenkiel, J.M. Nedeljkovic, Photoluminescence of anatase and rutile TiO_2 particles, J. Phys. Chem. B 110 (2006) 25366–25370.
[27] N. Serpone, D. Lawless, R. Khairutdinov, Size effects on the photophysical properties of colloidal anatase TiO_2 particles: size quantization or direct transitions in this indirect semiconductor?, J Phys. Chem. 99 (1995) 16646–16654.
[28] N. Zhang, R. Yi, L. Zhou, G. Gao, R. Shi, G. Qiu, X. Liu, Lanthanide hydroxide nanorods and their thermal decomposition to lanthanide oxide nanorods, Mater. Chem. Phys. 114 (2009) 160–167.
[29] E. Borgarello, J. Kiwi, M. Gratzel, E. Pelizzetti, M. Visca, Visible light induced water cleavage in colloidal solutions of chromium-doped titanium dioxide particles, J. Am. Chem. Soc. 104 (1982) 2996–3002.
[30] Cz. Koepke, K. Wisniewski, L. Sikorski, D. Piatkowski, K. Kowalska, M. Naftaly, Upconverted luminescence under 800 nm laser diode excitation in Nd^{3+} activated fluoroaluminate glass, Opt. Mater. 28 (2006) 129–136.
[31] J. Madhavan, P. Sathish Kumar, S. Anandan, F. Grieser, M. Ashokkumar, Degradation of acid red 88 by the combination of sonolysis and photocatalysis, Sep. Purif. Technol. 74 (2010) 336–341.
[32] P.R. Gogate, A.B. Pandit, A review of imperative technologies for wastewater treatment II: hybrid methods, Adv. Environ. Res. 8 (2004) 553–597.
[33] Z. Meng, L. Zhu, J. Choi, C.Y. Park, W. Oh, Sonocatalytic degradation of Rhodamine B in the presence of C60and CdS coupled TiO_2 particles, Ultrason. Sonochem. 19 (2012) 143–150.
[34] S. Sekar, M. Surianarayanan, V. Ranganathan, D.R. MacFarlane, A.B. Mandal, Choline-based ionic liquids-enhanced biodegradation of azo dyes, Environ. Sci. Technol. 46 (2012) 4902–4908.
[35] S. Sekar, S. Mahadevan, B.K. Shanmugam, A.B. Mandal, Bioenergetics and pathway of acid blue 113 degradation by *Staphylococcus lentus*, Biotechnol. Prog. 28 (2012) 1400–1408.
[36] A.G. Chakinala, P.R. Gogate, A.E. Burgess, D.H. Bremner, Intensification of hydroxyl radical production in sonochemical reactors, Ultrason. Sonochem. 14 (2007) 509–514.
[37] S.N. Katekhaye, P.R. Gogate, Intensification of cavitational activity in sonochemical reactors using different additives: efficacy assessment using a model reaction, Chem. Eng. Process. 50 (2011) 95–103.